JOURNAL OF GEOPHYSICAL RESEARCH, VOL. 106, NO. D19, PAGES 22,725–22,743, OCTOBER 16, 2001

A study of the dynamics of the equatorial lower stratosphere by use of ultra-long-duration balloons
1. Planetary scales

F. Vial,[1] A. Hertzog,[1] C. R. Mechoso,[2] C. Basdevant,[1] P. Cocquerez,[3]
V. Dubourg,[3] and F. Nouel[3]

Abstract. In the late southern winter of 1998, Centre National d'Études Spatiales (CNES), the French Space Agency, released six 10-m-diameter, superpressure balloons from a location near Quito, Ecuador. Three balloons collapsed soon after launching, but the remaining three drifted westward for a few weeks at altitudes between 19 and 20 km. Two of those balloons crossed the Pacific Ocean before falling above the "maritime continent," while the other completed a revolution around the Earth and crossed the Pacific for a second time before its final fall. Despite the small number and the relatively short duration of the flights, the balloons provided a unique in situ data set for the lower equatorial stratosphere. This part 1 of a two-part paper describes this data set and analyzes outstanding features in the planetary scales. Part 2 focuses on gravity-wave scale. It is argued that balloon trajectories over the Pacific are primarily determined by the westward drift during the easterly phase of the equatorial quasi-biennial oscillation (QBO) and the meridional velocity field of a mixed Rossby-gravity (Yanai) wave with an apparent period of 4 days and zonal wave number 4. This wave appears to have two episodes of amplification during the balloon flights. It is also argued that the balloons show evidence of oscillations with periods between 2 and 4 days and of a Kelvin wave with an apparent period close to 10 days and zonal wave number 1. In this way, the balloon behavior provided a pictorial view of air parcel trajectory in the equatorial lower stratosphere. It is stated that larger balloon campaigns can provide excellent in situ data sets for studies on the dynamics and composition of the middle atmosphere.

1. Introduction

Radio sounding balloons are the most commonly used observing system to systematically gather in situ data on the middle atmosphere. The system provides vertical profiles of wind and temperature at high spatial but low time resolutions. (In general, soundings are only made twice daily.) The distribution of radiosonde stations, however, is relatively sparse and features with strong horizontal gradients cannot be resolved. This is an important shortcoming, particularly since recent studies have emphasized the high dynamical relevance of strong gradients of Ertel's potential vorticity on isentropic surfaces [*McIntyre and Palmer*, 1984; *Plumb et al.*, 1994; *Mariotti et al.*, 1997]. Airplanes have been used to obtain in situ measurements with high spatial and temporal along-track resolutions in the lower stratosphere [*Plumb et al.*, 1994; *Carli et al.*, 2000; *Mariotti et al.*, 2000]. Airplane flights, however, cannot be more than a few hours long or reach locations too far away from land bases.

Balloons drifting at an approximately constant level in the lower stratosphere for weeks or months (i.e., ultra-long-duration balloons) can obtain in situ information relevant to the dynamics and composition of that region with very good temporal and spatial along-track resolutions. Plans to use ultra-long-duration balloons to perform horizontal soundings in support of studies on atmospheric dynamics were developed in the 1950s: *Lally* [1959] and *Giles and Angell* [1963], for instance, proposed the deployment of a fleet of such balloons to gather data for improvement of meteorological forecasts. These proposals resulted in the multiyear GHOST (Global Horizontal Sounding Technique) experiment [*Solot and Angell*, 1973], whose objective was to fill the gap in observations of the upper troposphere circulation in the Southern Hemisphere temperate latitudes. Later on, in 1975, 400 GHOST-type balloons were launched during the TWERLE (Tropical Wind Energy conversion and Reference Level Experiment) campaign [*Julian et al.*, 1977] and the collected data set was assimilated in the National Centers for Environmental Prediction (NCEP) reanalyses [*Kalnay et al.*, 1996].

[1]Laboratoire de Météorologie Dynamique, CNRS, Palaiseau, France.
[2]Department of Atmospheric Sciences, University of California, Los Angeles, California, USA.
[3]Centre National d'Études Spatiales, Balloon Division, Toulouse, France.

Paper number 2000JD000241.
0148-0227/01/2000JD000241$09.00

The French Space Agency (CNES) has had a long-term commitment to the use of balloons for studies on the dynamics and composition of the atmosphere. CNES has developed two types of ultra-long-duration balloons. The first is a superpressurized balloon (SPB), in which the lifting gas inside a closed envelope is kept at a pressure above the surrounding atmospheric pressure. In this way a SPB drifts quasi-horizontally at a constant density level. The second type is the infrared Montgolfière (MIR), an open balloon in which air is heated by solar radiation during daytime and infrared radiation emitted by Earth during nighttime [*Pommereau and Hauchecorne*, 1980; *Malaterre et al.*, 1995]. MIRs drift in the lower stratosphere. However, information provided by MIRs is somewhat difficult to interpret dynamically since the balloons make $\approx$ 5 km vertical excursions at sunset and sunrise. In 1971–1972 the Éole experiment carried about 500 flights with a 3.5-m-diameter CNES SPB to study the upper tropospheric (200 hPa) circulation in the Southern Hemisphere [*Morel and Bandeen*, 1973; *Sitbon*, 1975]. Some Éole balloons lasted for about 1 year, which demonstrated the reliability of CNES-SPB technology for the troposphere.

Exploration of the stratosphere, however, requires much larger SPBs than those used for the troposphere. This has motivated the development of new building technologies and operational procedures for handling the devices. Recent experiments such as electrodynamics of the middle atmosphere (EMA) [*Dowden and Holzworth*, 1990] or extended life balloon-borne observatories (ELBBO) [*Holzworth et al.*, 1993] have demonstrated that SPBs are able to fly for several months in the stratosphere. CNES has been developing an ambitious project to use ultra-long-duration SPBs to sample the lower southern stratosphere during spring, when the Antarctic "ozone hole" forms [*Vial et al.*, 1995]. The project name, Stratéole, reflects the motivation to extent the Éole's concept above the tropopause. Stratéole will use 10-m-diameter CNES SPBs capable of drifting for about 3 months between 50 and 70 hPa. The gondolas will carry instruments to sample the atmospheric state and composition, a Global Positioning System (GPS) receiver, and an ARGOS transmitter to deliver the data. The modern transmission and positioning technologies will allow a much more accurate and frequent determination of atmospheric parameters than during earlier experiments. Several preparatory campaigns are being carried out to assess the concept viability.

One preparatory campaign was held in the late southern winter of 1998, when CNES released six 10-m-diameter SPBs from Latacunga (72°W, 1°S) near Quito, Ecuador. (Hereinafter this effort will be referred to as "the Ecuador campaign.") The goals of the Ecuador campaign were primarily of a technological nature: (1) to certify the new SPBs in long-duration flights and (2) to estimate the maximum weight of gondolas that can be suspended from the hook of the balloons or, equivalently, their lowest reachable drifting level [*Dubourg et al.*, 1999]. Not all SPBs succeeded, but those that did gathered a highly interesting data set.

This paper and its companion [*Hertzog and Vial*, this issue] present an analysis of the data collected during the Ecuador campaign. Part 1 describes the campaign and focuses on the large-scale features of the flow. We examine the balloon trajectories and interpret their features in the context of equatorial wave dynamics. In particular, we claim that the Ecuador campaign provided a unique view of mixed Rossby-gravity-wave activity over the Pacific Ocean. This and other results justify the use of SPBs for studies on stratospheric dynamics.

We start in section 2 by presenting an overview of the Ecuador campaign. Section 3 discusses the balloon trajectories, how the horizontal velocities are obtained, and the vertical behavior of SPBs. Section 4 is dedicated to a Lagrangian analysis of the large-scale winds measured by the balloon. This analysis is complemented in section 5 from the Eulerian point of view, by looking at the operational radio sounding data set and at the analyses of the global circulation model from the European Centre for Medium-Range Weather Forecasts (ECMWF). Sections 6 and 7 give a summary of our main findings and of our conclusions. Part 2 [*Hertzog and Vial*, this issue] focuses on shorter-period gravity waves and examines the role of wave-mean flow interaction processes in the generation of the quasi-biennial oscillation (QBO).

2. Overview of the Ecuador Campaign

The CNES Stratéole balloon is a 10-m-diameter SPB with a 50-μm-thick envelope made of bilaminated polyester film. Helium is used as the lifting gas. Once at its drifting level, the SPB lifetime is limited only by helium effusion through the envelope or by loss through microleaks. For a 2-month-duration flight, the equivalent leak diameter must not exceed a few tenths of millimeters. The gondola consists of polystyrene tubes covered with aluminized polyester that allows the thermal conditioning of different elements. The energy for onboard instrumentation is provided by lithium batteries. For a nominal flight level around 50 hPa the balloon can carry a 20 kg weight.

Six Stratéole SPBs (SPB1-SPB6) were released during the

Table 1. SPB Flights Characteristics During the Ecuador Campaign

SPB	Launch	End	Duration (day)	$\bar{P}$ (hPa)	$\bar{z}$ (km)
1	25/8 (237)[a]	13/9 (256)	20	58.1	19.9
2	1/9 (244)	17/10 (290)	47	57.9	19.9
5	7/9 (250)	30/9 (273)	24	65.0	19.3

[a] Julian days in 1998.

Ecuador campaign. The basic instruments in the gondolas were two temperature sensors, a pressure sensor, a GPS receiver, and an ARGOS transmitter. The helium temperature and pressure were also monitored. All measurements were made every 12 min. Only three flights lasted for more than few days: SPB1, SPB2, and SPB5 launched August 25, and September 1 and 7, 1998, respectively. The characteristics of these flights are summarized in Table 1. Note that SPB5 had a heavier gondola, a lower drifting level (600 m), and a slower speed than SPB1 and SPB2. Concerning the other SPBs, the gondola of SPB3 was too heavy, which induced an excessive discrete load and caused the balloon to explode as it reached drifting level. SPB4 was lost due to failure of the electrical power system of the gondola, but the balloon behavior was nominal for 4 days after the launch. SPB6, another attempt with heavy payload, was lost in less than 1 day due to leaks in the envelope. More details on the campaign are given by *Dubourg et al.* [1999].

The absolute and relative accuracy of the pressure sensor used in the Ecuador campaign are about 1 hPa and 0.1 hPa respectively. Thus pressure variations can be used to gain insight into the vertical motions of air parcels around the gondola. This method should be applied with caution to SPB5, since pressure fluctuations for this balloon were overestimated due to a calibration problem. On the other hand, the errors in GPS positioning are estimated to be 100 m in both vertical and horizontal directions.

The daytime temperatures obtained by the atmospheric sensors are not reliable because the sensors themselves were exposed to absorption of solar radiation. Furthermore the sensors were too close to the gondola and could be from time to time in its wake. Thus only the nighttime air temperature data are used in the present analysis.

The first step in the data analysis was quality control. Spurious data resulted, in most cases, from problems during the data transmission or reception via the Argos satellites. The criteria for rejection was based on a close inspection of the consistency with values at nearby locations. Vertical position and temperature measurements were too noisy to serve as selection criteria. Missing data points (either not received by the Argos ground stations or eliminated during the quality-control process) were obtained by interpolation using the method of cubic splines. They represented nearly 15% of the total amount of data, of which 65% were isolated cases. Our procedure for filling data gaps is therefore not expected to produce systematic errors.

3. Balloon Trajectories, Horizontal Velocities and Vertical Displacements

SPB1, SPB2, and SPB5 flew during 20, 47, and 24 days, respectively. This section describes their trajectories and behavior in the vertical.

3.1. Trajectories and Horizontal Velocities

Figure 1 displays the trajectories of the three flights. Since the equatorial quasi-biennial oscillation was in its easterly phase in 1998, all the SPBs drifted westward across the Pacific Ocean. SPB1 and SPB5 fell down over the "maritime continent" when passing over very cold convective systems during nighttime. SPB2 made one complete turn around the world and crossed the Pacific again before falling over Indonesia in similar circumstances. Over the Pacific, all balloons exhibited large oscillations around the equator. These were weaker in the second pass of SPB2 over the Pacific, and the device remained north of the equator. A striking feature in Figure 1 is the almost superposition of the three trajectories west of South America. We shall return to this point later in the text. Note, finally, that the SPBs always flew in the equatorial stratosphere and that none escaped to the midlatitudes. The dynamical isolation of the equatorial lower stratosphere indeed prevent such meridional transport [e.g., *Dunkerton*, 2000].

If λ_i (λ_{i+1}) and θ_i (θ_{i+1}) are the longitude and latitude of the balloon provided by the GPS at time t_i (t_{i+1}), then the zonal (u_i) and meridional (v_i) components of the balloon velocities at time t_i are approximately given by

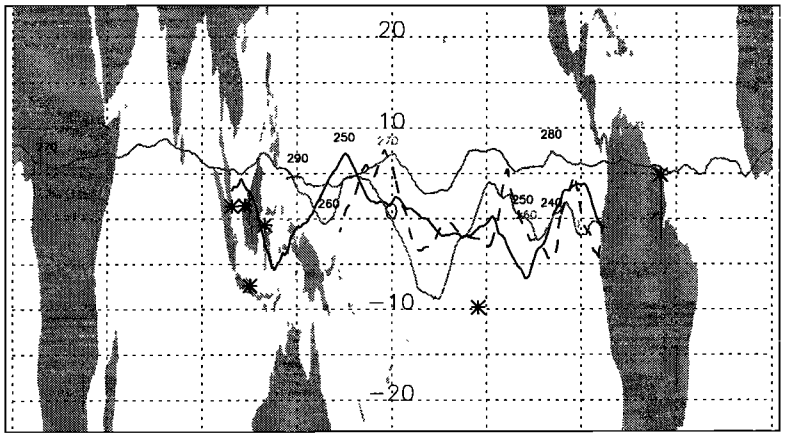

Figure 1. Trajectory of the balloons (SPB1, solid curve; SPB2, solid grey; SPB5, dashed). The labels on the trajectories indicate Julian days (in 1998). Radio sounding stations used in this study are marked with asterisks.

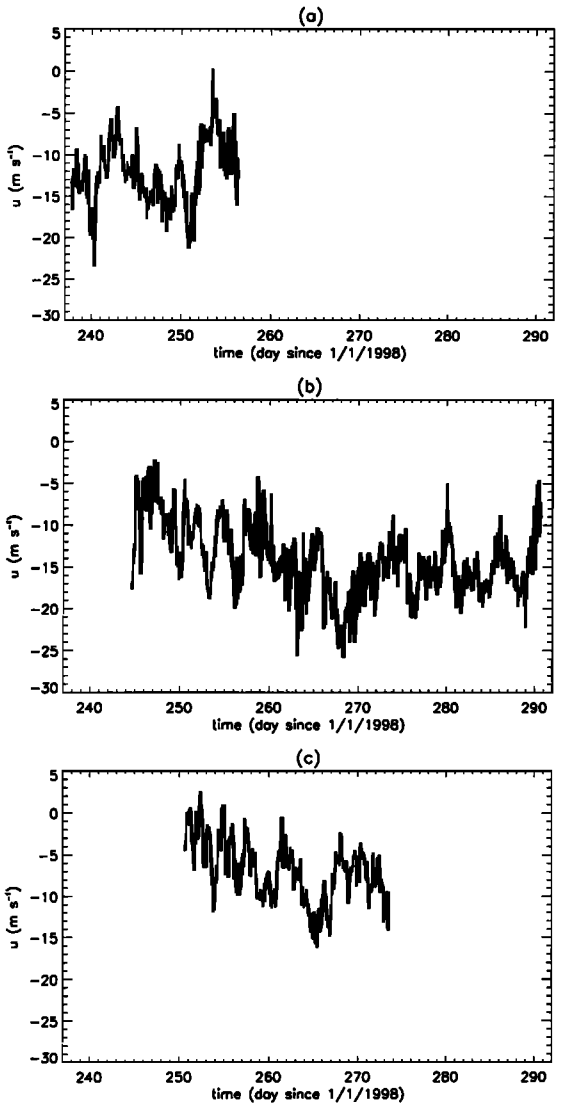

Figure 2. Zonal wind (positive eastward) estimated by (a) SPB1, (b) SPB2, and (c) SPB5.

$$u_i = R\cos\theta_i \frac{\lambda_{i+1} - \lambda_i}{t_{i+1} - t_i}, \tag{1}$$

$$v_i = R\frac{\theta_{i+1} - \theta_i}{t_{i+1} - t_i}, \tag{2}$$

where R is the radius of the Earth.

The error made in the calculations of horizontal velocities according to equations (1) and (2) is $\Delta u = \sqrt{2}\Delta x/\Delta t$, where Δx is the error in horizontal GPS positions and $\Delta t = t_{i+1} - t_i$. If an upper bound for Δx is 100 m and $\Delta t = 720$ s, then the error in the balloon velocity is much less than 1 m s^{-1}. On the other hand, no information on the balloon vertical velocities can be deduced using GPS data since the vertical displacements of the balloons and the GPS accuracy are of the same order. In the remainder of this paper we will assume that horizontal balloon velocities are a good approximation of horizontal wind velocities. (Appendix A discusses the validity of this assumption.)

The zonal and meridional wind velocities for the three balloon flights are displayed in Figures 2 and 3, respectively. In all cases both velocity components display fluctuations at several timescales. The along-track averaged zonal wind velocities of SPB1 and SPB2 are -12.1 m s^{-1} and -14.1 m s^{-1}, respectively. The small difference between these values appears because SPB1 drifted approximately along the equator, while SPB2 behaved similarly during its first pass over the Pacific but drifted approximately along 5°N during its second pass. The along-track zonal wind velocity of SPB5 is -7 m s^{-1}. SPB1 and SPB2 drifted at about 7 hPa lower than SPB5 and the vertical gradient of the zonal wind was about 1 m s^{-1} hPa^{-1} (≈ -10 m s^{-1} km^{-1}) according to radiosonde data (see section 5.1). On the other hand, the along-track averaged meridional wind component is practically zero in all cases.

The fluctuations with a few days period, present in the meridional wind components, clearly reflect the large oscillations in the trajectories. Other oscillations with longer

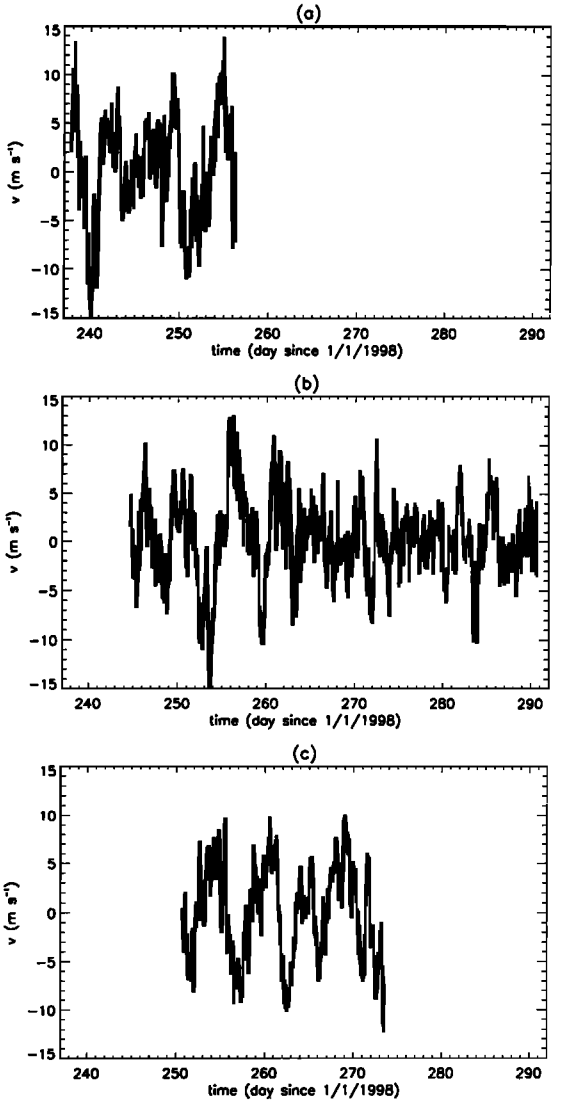

Figure 3. As in Figure 2 except for the meridional wind (positive northward).

timescales are apparent only on the zonal velocities. This is particularly clear for SPB2, whose flight duration was longer than the other SPBs.

3.2. Balloon Vertical Displacements

Balloons would move exactly on a particular isopycnal surface if their envelopes were rigid and had no leak. Envelopes can slightly contract or expand, however, and can have leaks. The result is a change in isopycnal surface and drifting level. This is better discussed in terms of the superpressure (P_s) defined as

$$P_s = P_h - P_a\,, \tag{3}$$

where P_h and P_a are the helium and surrounding air pressures, respectively. Changes in P_s result in changes in the envelope volume and thus variations in the balloon drifting level (see Appendix B).

In short, for a "no-leak" envelope, P_h can change as the helium temperature increases or decreases when the envelope warms up or cools down in response to variations in impinging radiation. Such variations are induced by the balloon going from day-to-night conditions (and vice versa) or by other effects, notably the passage of the device above very cold convective superclusters. P_a, on the other hand, can vary on isopycnal surfaces. Appendix B shows that the vertical balloon excursions associated with the effects listed are generally too small to be detected by the GPS and induce a very weak contamination of the air pressure record. Finally, leaks in the envelope can also induce small trends in altitude changes.

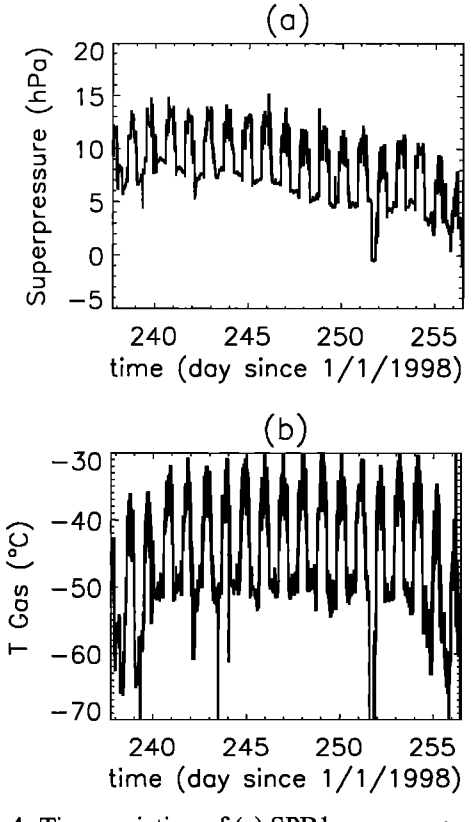

Figure 4. Time variation of (a) SPB1 superpressure and (b) helium temperature.

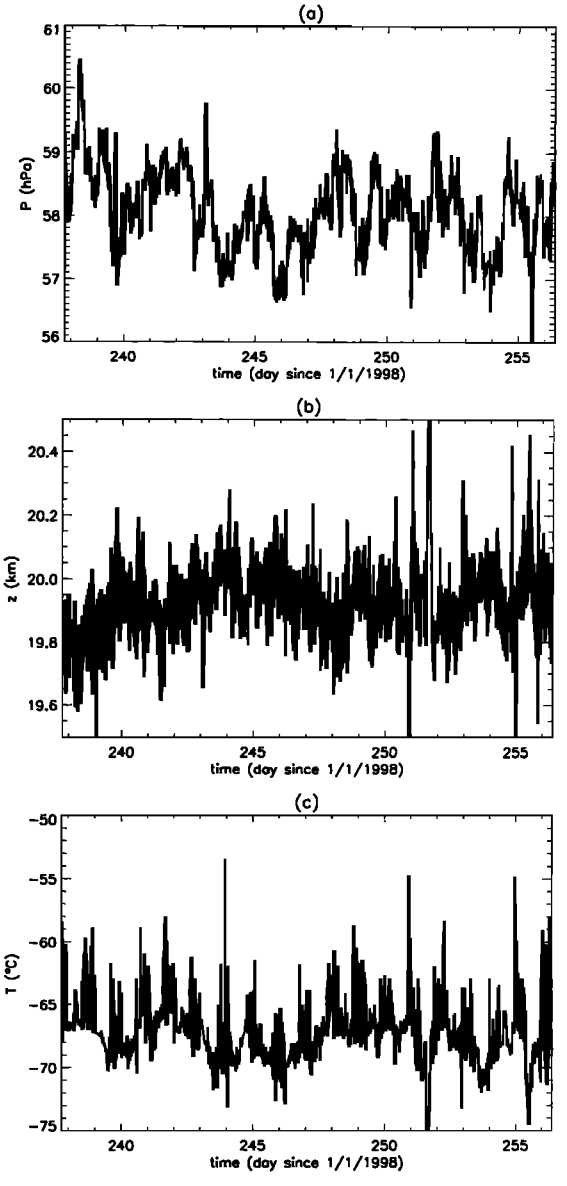

Figure 5. Time variations of (a) air pressure, (b) altitude, and (c) air temperature recorded by SPB1.

Figures 4a and 4b present the time variations of superpressure and helium temperature for SPB1. The decreasing trend of the superpressure indicates helium loss due to microleaks in the envelope which were almost certainly generated during the launching procedure. These leaks, with an estimated total diameter of 0.22 to 0.48 mm, ultimately limited the lifetime of the balloon, whose end was accelerated by its pass over a cold convective system. The superpressure and helium temperature in Figure 4 also show a diurnal cycle, with larger values during daytime.

As stated earlier, changes in superpressure have small consequences. One notable exception to this systematic behavior, however, was found on September 8 (day 251), when SPB1 was northeast of Borneo passing above a very cold convective system. The strong nighttime cooling of the

balloon envelope and helium were not compensated by the weak infrared emission from below. As a consequence, the helium temperature greatly decreased, pressure inside the envelope became eventually smaller than the atmospheric pressure, and the balloon shrunk and dropped around 1.5 km for about 4 hours. When the Sun rose again, the helium warmed and the balloon climbed back to its nominal drifting level. SPB1 (as well as SPB2 and SPB5) finally collapsed during the night above similar very cold cloud systems. The data gathered during day 251 will be considered separately in the following because the large vertical excursion of the balloon could contaminate other signals.

Figure 5 show time variations of air pressure, GPS altitude, and nighttime air temperature, respectively, obtained during the SPB1 flight. The pressure shows fluctuations in all timescales with magnitudes up to 3 hPa in a few days. Low-frequency (a few days) pressure and altitude fluctuations are clearly anticorrelated. Instantaneous altitude measurements, on the other hand, are noisy and do not clearly reflect any atmospheric process. Low-frequency temperature and pressure fluctuations are positively correlated as the balloon drifted on a nearly isopycnic surface.

4. Lagrangian Analysis of the Large-Scale Dynamics

4.1. Spectral Analysis

Figure 6 displays for the three flights the low-frequency part (up to 4 cycles d^{-1}) of the power spectra of the two horizontal wind components and pressure. (The high-frequency portion of the spectra will be discussed in part 2 of this paper.) To produce Figure 6, we used the standard multitaper method [*Percival and Walden*, 1993]. Calculations were made for the entire duration of the flights, and therefore the spectral resolution is different for each case. The error bars that correspond to the 90% confidence level, constant on a log plot, are shown for the lowest frequency. The estimated noise level associated with the GPS measurements reaches a magnitude comparable with the wind signal at frequencies much higher (30 cycles d^{-1}) than those plotted (see Figure 2 of part 2).

The power spectra of pressure for SPB2 and SPB5 show sharp peaks at (or very close to) 1 cycle d^{-1}; the spectrum of pressure for SPB1 exhibits a weaker peak around that frequency. As discussed in section 3, such peaks result from the day-night vertical excursions of the balloons. There is no clear indication of similar peaks in the plots for the horizontal wind components. This is understandable since vertical gradients in horizontal winds are much smaller than in pressure.

At lower frequencies the power spectrum of pressure for SPB2 shows largest values around 0.1 cycle d^{-1}. This feature does not have a counterpart in the records for SPB1 and SPB5, whose flights are too short to clearly resolve that frequency.

In all cases the power spectrum for the meridional wind shows the largest values around 0.2 cycles d^{-1}. This corresponds to the period of the large oscillations around the equator visible on the balloon trajectories over the Pacific (see Figure 1). At frequencies lower than 0.1 cycle d^{-1} the spectral power of the meridional wind for SPB2 is smaller than for the zonal wind. On the other hand, at frequencies higher than 0.1 cycle d^{-1} the spectral power of the meridional wind for SPB1 and SPB5 tends to be larger than for the zonal wind. This is less clear for SPB2, which encountered different dynamical situations since its duration was longer. Some other peaks seem to emerge also at periods between 0.1 and 1 cycle d^{-1}.

4.2. Wavelet Analysis

The balloons observations are clearly nonstationary. For instance, the SPB2 large meridional excursions visible above the Pacific have no counterpart elsewhere. Thus we complement the results presented in the previous subsection with a wavelet analysis, which examines wave activity in the time-frequency domain.

Our wavelets $\psi_{j,n}(t)$ are of the Battle-Lemarié type. Besides, we select complex (analytic) wavelets in order to recover the phase of the fluctuations [*Mallat*, 1998]. The real and imaginary parts of the "mother wavelet" ($\psi(t)$) are shown in Figure 7. The mother wavelet can be dilated to analyze details of the signal with larger scales and translated along the time axis to cover the entire time range of the data. The different analyzing windows are linked to the mother wavelet through

$$\psi_{j,n}(t) = j^{-1/2}\psi\left(\frac{t-t_n}{j}\right) , \qquad (4)$$

where j is the scale factor and t_n is the nth measurement point. The decomposition of a signal $s(t)$ onto this set of functions is given by

$$\tilde{s}_{j,n} = s(t) \star \psi_{j,n}(t) , \qquad (5)$$

where the star stands for the convolution product.

Plates 1 and 2 display the squared modulus of the wavelet decomposition applied to the zonal ($|\tilde{u}_{j,n}|^2$) and meridional ($|\tilde{v}_{j,n}|^2$) wind components and pressure for SPB2, and SPB1 and SPB5, respectively. The spectral signatures we encountered in the simple Fourier transform are more clearly evidenced in this decomposition.

For SPB2, which had the longest flight, the most striking feature is the maximum in the meridional wind activity between days 250 and 260 with periods around 5–7 days, when the balloon was above the central Pacific and its trajectory experienced large meridional excursions. Simultaneously, the zonal wind and pressure exhibit increased activity with periods around 3–4 days. After day 261, SPB2 drifted at about 5°N. During this period, the meridional wind shows three other episodes of increased activity. The first is around day 262 with periods around 3–4 days, when the balloon passed above the eastern Indian Ocean. The second episode is around day 271 with periods around to 2 days, when SPB2 passed above western Africa and the eastern Atlantic Ocean.

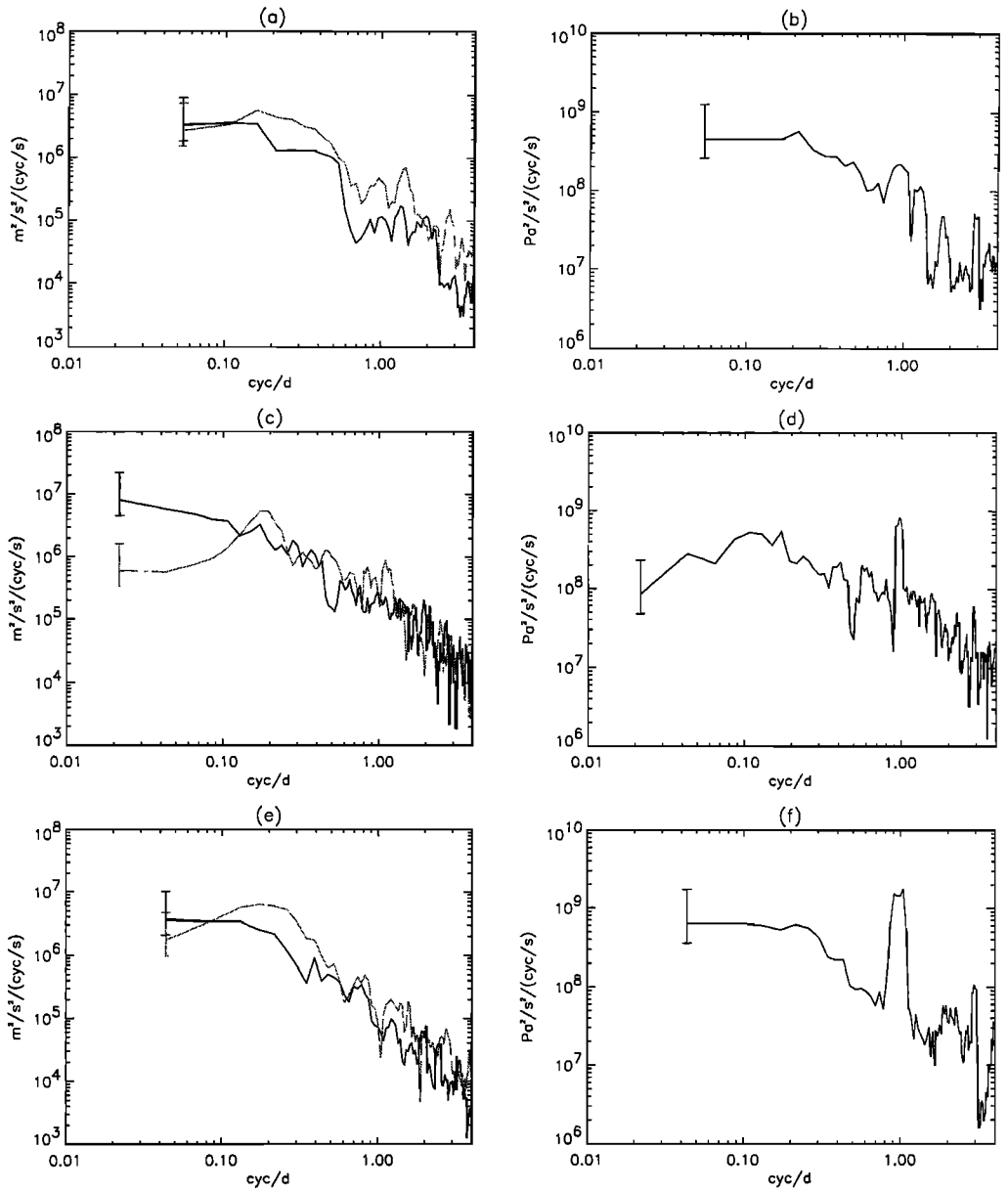

Figure 6. Spectrum of the zonal (black) and meridional (grey) wind fluctuations (a, c, and e) and pressure fluctuations (b, d, and f) obtained with SPB1 (top), SPB2 (middle) and SPB5 (bottom).

The last episode of increased meridional wind activity is between days 281 and 289 with periods of about 4 days, when the balloon passed over the eastern Pacific Ocean for the second time. Concerning the zonal wind and the pressure, with the exception of the period between days 250 to 260 mentioned above, most activity is at periods around 6–8 days and longer.

The shorter lifetimes of SPB1 and SPB5 do not allow to extend the wavelet analysis to periods greater than 5 days, which precludes consideration of long-period oscillations. Nevertheless, Plate 2 gives complementary information on the oscillations discussed with SPB2 data.

For SPB1 the meridional wind shows increased activity before day 245 and after day 250, at periods longer than 5 days, when the balloon was above the western Pacific. The zonal wind shows increased activity before day 245 and largest values after day 250, with periods around 4 days in both cases. Note the similarity between the results for SPB2 and SPB1 between days 250 and 255, where the former was over the central Pacific and the latter over the western Pacific.

For SPB5, which only flew over the Pacific, the meridional wind shows enhanced activity from day 250 to day 265 at period longer than 5 days. There is another period of increased meridional wind activity around day 271 with periods around 2 days, when the balloon was approaching Indonesia. A similar feature was obtained by SPB2 at the same time. Notice, finally, that all the transient periodic oscillations we described above have weak but still visible signatures in the power spectra presented in section 4.1.

4.3. Lagrangian Versus Eulerian Framework

This section examines the extent to which the Lagrangian information given by the SPBs can be interpreted in the Eulerian framework. To start with, let us assume that SPBs are perfect Lagrangian tracers. Since the SPBs drifted at a constant density level, we can, without loss of generality, restrict ourselves to a two-dimensional (2-D) horizontal motion.

The quasi-sinusoidal pattern of balloon trajectories over the Pacific Ocean (see Figure 1) suggests the existence of substantial planetary wave activity. In the simplest scenario, we could describe the flow as the superposition of a mean zonal wind $\bar{u}$ plus a wave in the meridional velocity with no latitudinal structure:

$$u = \bar{u}\,, \tag{6}$$

$$v = v_0 \sin(s\lambda - \omega t)\,, \tag{7}$$

where v_0, s, and ω are the wave amplitude, zonal wave number, and frequency relative to the ground (i.e., apparent frequency). Since the balloons are advected in the east-west direction by the mean zonal wind ($\lambda_{\text{bal}} = \frac{\bar{u}t}{R}$, where R is the Earth radius), the frequency of their meridional excursions in the mean wind reference frame (i.e., intrinsic frequency) is given by

$$\omega_0 = \omega - \frac{\bar{u}s}{R}\,. \tag{8}$$

Alternatively, the oscillations can be viewed as having an "intrinsic wave number" (s^*) given by

$$s^* = s - \frac{R\omega}{\bar{u}}\,. \tag{9}$$

A Lagrangian analysis of the type performed so far, therefore, only allows us to determine ω_0 (or s^*). In this regard, the spectrum and wavelet analysis of the meridional velocities estimated by SPB1, SPB2, and SPB5, finds peaks at frequencies of about 0.2 cycles d^{-1} and 0.5 cycles d^{-1}, whereas that of zonal velocity finds a peak at 0.1 cycle d^{-1}.

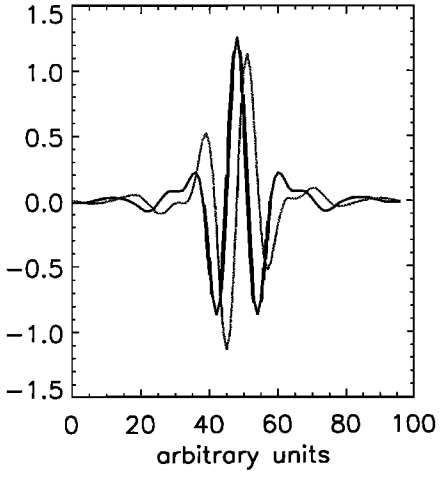

Figure 7. Real (black) and imaginary (grey) part of the Battle-Lemarié wavelet.

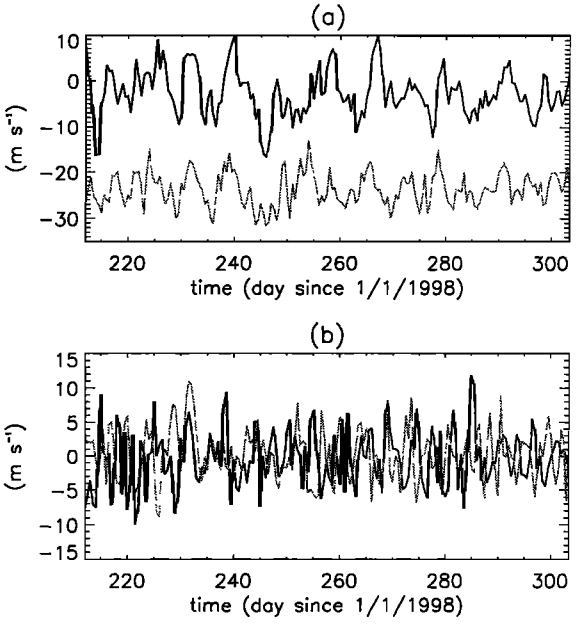

Figure 8. (a) Zonal and (b) meridional wind components from radiosondes launched twice daily from Singapore during the period August 1 to October 31, 1998 (black curve, 70 hPa; grey curve, 50 hPa).

On the other hand, the analyses do not allow us to uniquely determine the planetary wave parameters ω and s.

5. Ancillary Data Sets

A large number of balloons drifting simultaneously would certainly allow to fully document the wind field. For instance, *Desbois* [1975] has shown that it was possible to infer the characteristics of planetary waves in the upper troposphere with the Éole data set. However, in this study we only dispose of three balloons. Therefore in this section, we appeal to other observational data sets to gain further insight into the equatorial planetary waves during the flights of SPB1, SPB2, and SPB5. The data sets selected are routine radio soundings, made at stations close to the equator, and the global analyses made at the ECMWF.

5.1. Radiosondes

We use twice-daily radiosonde data to obtain an estimate of frequencies and length scales of disturbances in the lower stratosphere during the Ecuador campaign. The data correspond to six stations: Singapore (1.4°N, 104°E), Kuching (1.5°N, 110.3°E), Rochambeau (4.8°N, 52.4°W), Surabaya (7.4°S, 112.8°E), Palu (0.7°S, 119°E), and Marquises Islands (9.8°S, 139°W). Since the SPBs drifted at about 60 hPa, we restrict our analysis to the nearest standard levels above and below: 50 and 70 hPa. Values when data were missing were obtained by linear interpolation between nearest adjacent points. This interpolation could result in artificial spectral peaks for the three stations in the Southern Hemisphere, whose data sets have many gaps.

The horizontal wind components at 50 hPa and 70 hPa recorded at Singapore between August 1 (day 213) and Oc-

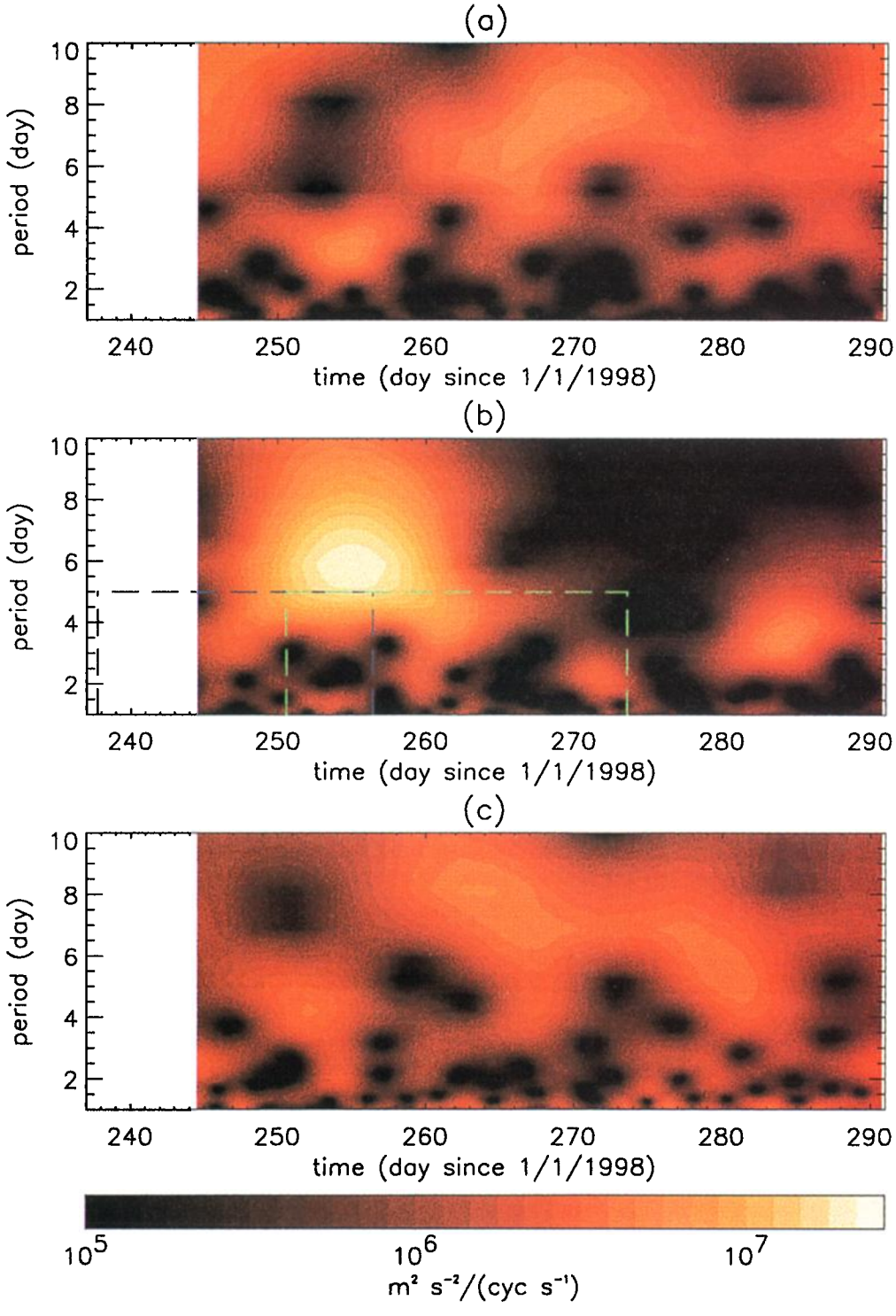

Plate 1. Wavelet analysis of (a) the zonal wind, (b) meridional wind, and (c) pressure fluctuations for SPB2. The pressure fluctuations have been magnified by a factor of 10. Dashed lines in the middle panel show the time-frequency domain analyzed for SPB1 (blue) and SPB5 (green). The color code is shown at the bottom of the plot.

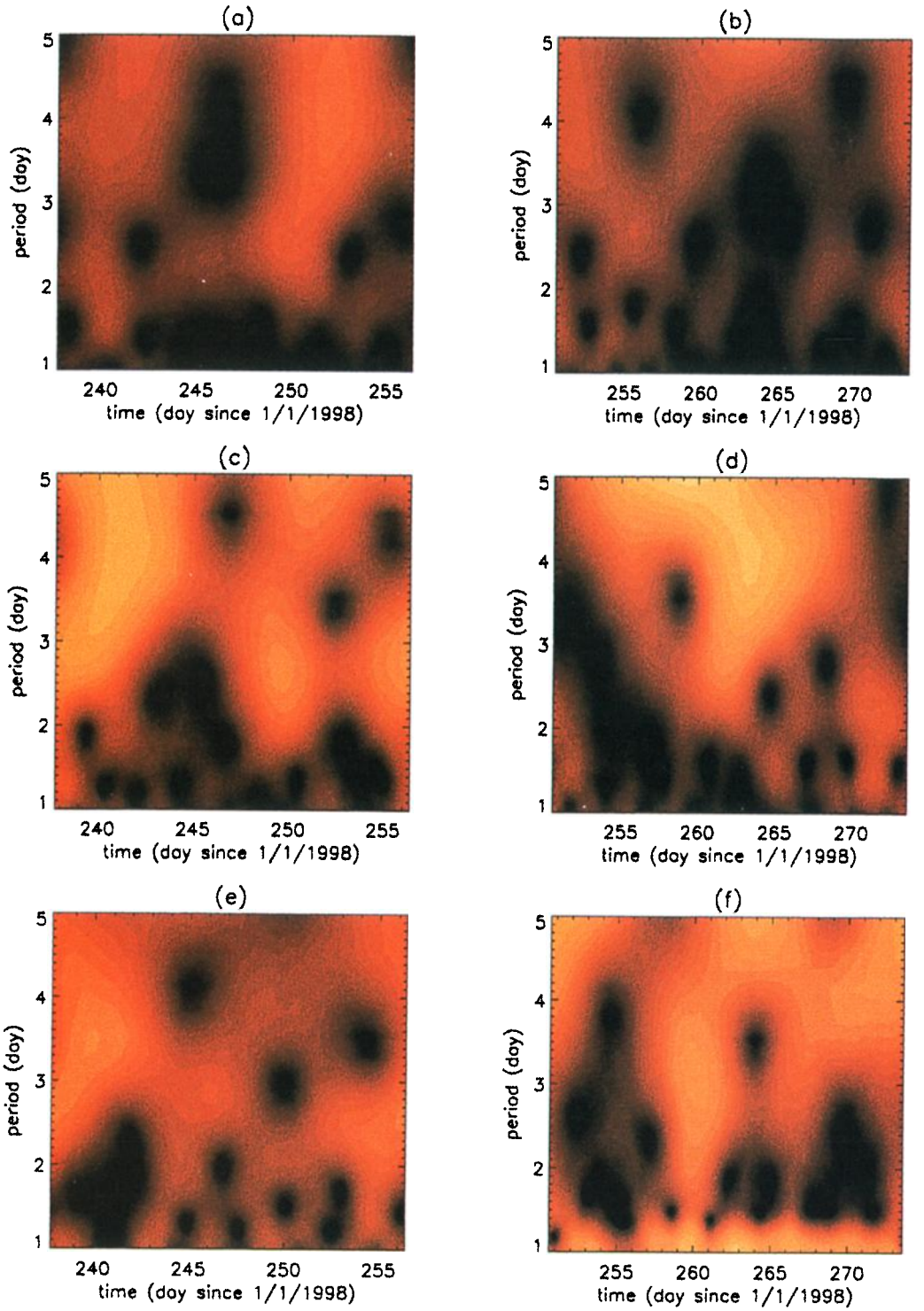

Plate 2. As in Plate 1, except for SPB1 (left) and SPB5 (right).

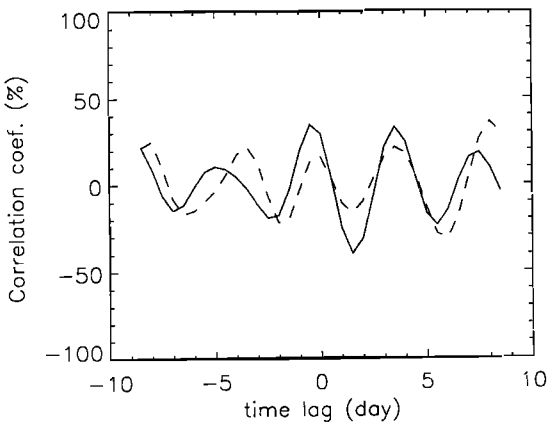

Figure 9. Cross correlations of the meridional wind at 70 hPa between Singapore and Palu (solid), and Singapore and Rochambeau (dashed). Negative time lag means that Singapore lags the other stations. The westward 4-day wave dominates the signal in the meridional wind and induces symmetric disturbances about the equator.

tober 31 (day 304) are shown in Figure 8. The differences in zonal winds between those levels are consistent with the vertical structure of the QBO during the selected period. It is apparent that the meridional wind exhibits oscillations at rather short periods (a few days), whereas the zonal wind exhibits larger oscillations at longer periods. A spectral analysis of these time series (not shown) reveals significant peaks for most of the six stations in the 3 to 5-day band and in the 8 to 12-day band. We will refer to the oscillations represented by those peaks as the 4-day and the 10-day wave, respectively.

For the stations very close to the equator, the amplitude of the 4-day wave in the meridional wind component is much larger than in the zonal one. On the other hand, in all the stations, the amplitude of the 10-day wave in the zonal wind component is much larger than in the meridional one.

The phase differences between stations enabled us to infer the horizontal wavelengths of those wave signal. This is illustrated in Figure 9, which present the cross correlations of the meridional wind at 70 hPa between Singapore, Palu, and Rochambeau. It is found that the 4-day wave propagates westward, whereas the 10-day wave propagates eastward. The phase speeds are about –22.5° d^{-1} (−29 m s^{-1}) for the 4-day wave and 40° d^{-1} (50 m s^{-1}) for the 10-day wave, which correspond to zonal wave numbers 4 and 1, respectively.

The analysis of the 4-day wave phase in both hemispheres shows that the meridional wind component is primarily symmetric about the equator, whereas the zonal one is primarily antisymmetric whatever the level. In contrast, the zonal wind component of the 10-day wave was found to be symmetric about the equator. The amplitude of both waves are larger at 70 hPa than at 50 hPa.

These characteristics agree with the notion that the 4-day wave with zonal wave number 4 corresponds to the mixed Rossby-gravity wave, which was described for the first time by *Yanai and Maruyama* [1966]. They also suggest that the 10-day wave with zonal wave number 1 corresponds to the Kelvin wave described by *Wallace and Kousky* [1968].

We can now use equation (8) to examine whether the waves captured in the analysis of radiosonde data have a signature in the results obtained in the spectral and wavelet analyses of SPB data. According to Figure 2, we can take $\bar{u} \approx -15$ m s^{-1}. For the mixed Rossby-gravity wave, the apparent period is 3–5 days that, according to equation (8), yields an intrinsic period of 5–8 days. The most prominent features in the spectral and wavelet analyses of the meridional wind were found in that period band. Similarly, for the Kelvin wave, an apparent period in the radio soundings of 10 days yields an intrinsic period of 7.5 days. Again, the most prominent feature in the spectral and wavelet analyses of the zonal wind and pressure was found around this period.

5.2. Idealized Balloon Trajectories

We have seen in the wavelet analysis of SPB1 and SPB2 data (section 4.2) that enhanced meridional wind activity with periods around 5–7 days appears associated with enhanced zonal wind and pressure activity at periods around 3–4 days. To qualitatively demonstrate that this feature is consistent with the signature of a mixed Rossby-gravity wave with an apparent period of about 4 days and a zonal wave number equal to 4, let us consider the zonal and meridional wind perturbations induced by such a wave. These can be expressed at a given altitude as [*Andrews et al.*, 1987]

$$u' = -A\frac{|m|\omega_0 y}{N} e^{-\frac{\beta|m|y^2}{2N}} \sin(s\lambda - \omega t + \phi_0)\,, \quad (10)$$

$$v' = A\, e^{-\frac{\beta|m|y^2}{2N}} \cos(s\lambda - \omega t + \phi_0)\,, \quad (11)$$

where s and m are the horizontal and vertical wave numbers, ϕ_0 is the phase at $t = 0$, N is the Brunt-Väisälä frequency, and y is the meridional coordinate in the equatorial beta plane. The vertical wave number of the wave satisfies the dispersion relationship:

$$m = \frac{N}{\omega_0^2}\left(\beta + \omega_0 \frac{s}{R}\right). \quad (12)$$

If $N^2 = 6 \times 10^{-4}$ radian^2 s^{-2} (a mean value deduced from the radiosonde data analyzed in section 5.1), then $m = 2.5$ cycles km^{-1}. The time variations of the longitude and latitude of a SPB in the wind field given by a zonal flow $\bar{u}$ plus a perturbation of the form given by equations (10) and (11) satisfy

$$a\cos\theta \frac{D\lambda}{Dt} = \frac{Dx}{Dt} = \bar{u} + u'\,, \quad (13)$$

$$a\frac{D\theta}{Dt} = \frac{Dy}{Dt} = v'\,. \quad (14)$$

(Note that the vertical displacements of the isopycnic surfaces due to the disturbance are much less than the vertical

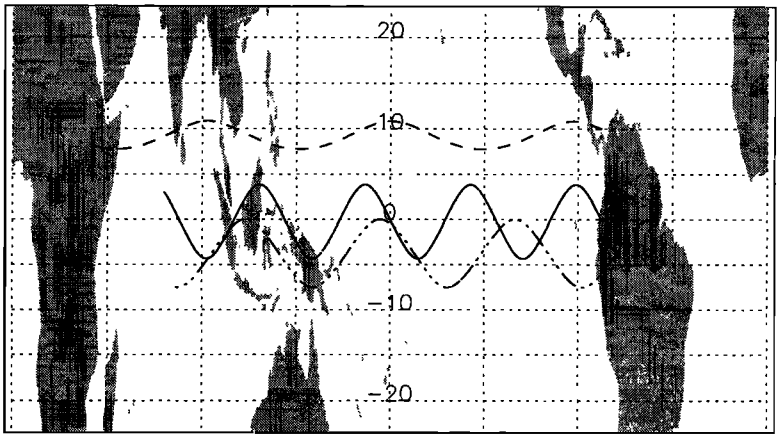

Figure 10. Idealized trajectories of Balloons 1 (solid), 2 (dotted-dashed), and 3 (dashed). The wind field consists of a constant zonal background wind ($\bar{u} = -15$ m s^{-1}) and a Rossby-gravity wave with a zonal wave number of 4, an intrinsic frequency of $-1/6$ cycle d^{-1} and an amplitude of the meridional wind at the equator of 7 m s^{-1}. Initially, Balloons 1 and 2 are at the equator, whereas Balloon 3 is at 10° N.

wavelength of the wave, so it can be assumed that SPBs drift at approximately constant altitudes.) To solve these equations, we take $A = 7$ m s^{-1} and $\bar{u} = -15$ m s^{-1}, which correspond roughly to the amplitude of the Rossby-gravity wave above the Pacific Ocean and to the mean zonal wind during the SPB flights. Figure 10 shows three solutions of equations (13) and (14) obtained using the fourth-order Runge-Kutta integration scheme. We will refer to these solutions as the trajectories of "Balloons" 1, 2, and 3. Initially, Balloons 1 and 2 are at the equator, while Balloon 3 is at 10° N.

Depending on the wave phase at the initial time, the trajectories initiated at the equator either cross it during the simulation (Balloon 1) or remain to one side of it (Balloon 2). Balloon 3, which was launched at 10° N, does not find large enough meridional wind to cross the equator. It indeed feels larger zonal-wind disturbances than meridional ones.

The variations with time of the zonal and meridional velocity components along the idealized trajectories are shown in Figure 11. As expected, the meridional wind exhibits oscillations with periods close to 6 days (i.e., the intrinsic period of the Rossby-gravity wave). The zonal wind fluctuations are, however, quite different for each case. In particular, Balloon 1 exhibits higher-frequency oscillations that are also captured by Balloon 2, though to a weaker extent, and which are missed by Balloon 3. This behavior is due to the antisymmetric structure about the equator of the zonal wind induced by Rossby-gravity waves. Thus when Balloon 1 crosses the equator, the zonal wind exhibits a phase jump of half a period, which is responsible for the higher-frequency oscillations of this component. The weaker oscillations seen on Balloon 2 are due to the fact that the wave component of the zonal wind vanishes at the equator. In contrast, zonal-wind oscillations of Balloon 3 look very similar to those of the meridional wind, since this balloon always stays away from the equator.

These calculations reveal several features of interest. The wave amplitude (for instance, the amplitude of the meridional wind at the equator) may be underestimated by the balloon velocity (see Balloon 2). Oscillations in the zonal wind with a frequency different from the intrinsic frequency of the wave appear if the balloon crosses the equator.

Finally, the mean zonal wind is not necessarily well determined not only because of the meridional excursion of the balloon but also because of the balloon Stokes drift $\bar{u}^s$. For a Rossby-gravity wave, the Stokes drift for $\bar{u}$ linear in z is given by [*Andrews et al.*, 1987]

$$\bar{u}^s = \frac{1}{2}\left(\frac{m}{N} - \frac{2m^2\beta y^2}{N^2}\right) e^{-\frac{\beta m y^2}{N}} A^2 . \qquad (15)$$

Thus the Stokes drift is eastward close to the equator: at the equator the theoretical value is $\frac{m}{2N}A^2 = 2.5$ m s^{-1}. The Stokes drift for Balloons 1 and 2 are 1.6 m s^{-1} and 0.4 m s^{-1}, respectively, since they do not stay at the equator. Poleward of $y = \sqrt{\frac{N}{2m\beta}}$ (i.e., $\approx 4°$ in our calculations), the Stokes drift is westward. The value corresponding to Balloon 3 is -0.9 m s^{-1}.

5.3. ECMWF Analysis

In this section we examine the analysis fields produced during the Ecuador campaign by ECMWF. This is done for two reasons. First, analysis fields can provide a more global picture of the circulation in the equatorial lower stratosphere. Second, in situ SPB data can provide an analysis validation in the poorly sampled equatorial stratosphere. The ECMWF fields are available every 6 hours (0000, 0600, 1200, 1800 UT) on a $1.125° \times 1.125°$ horizontal grid. There are 31 levels in the vertical, six of which are in the equatorial stratosphere, and the vertical resolution near the SPB drifting level is roughly of 2 km. We used cubic splines in time and space to interpolate the analysis fields to the SPB positions.

A comparison between the horizontal wind components and the temperature from SPB1 and the ECMWF analysis is

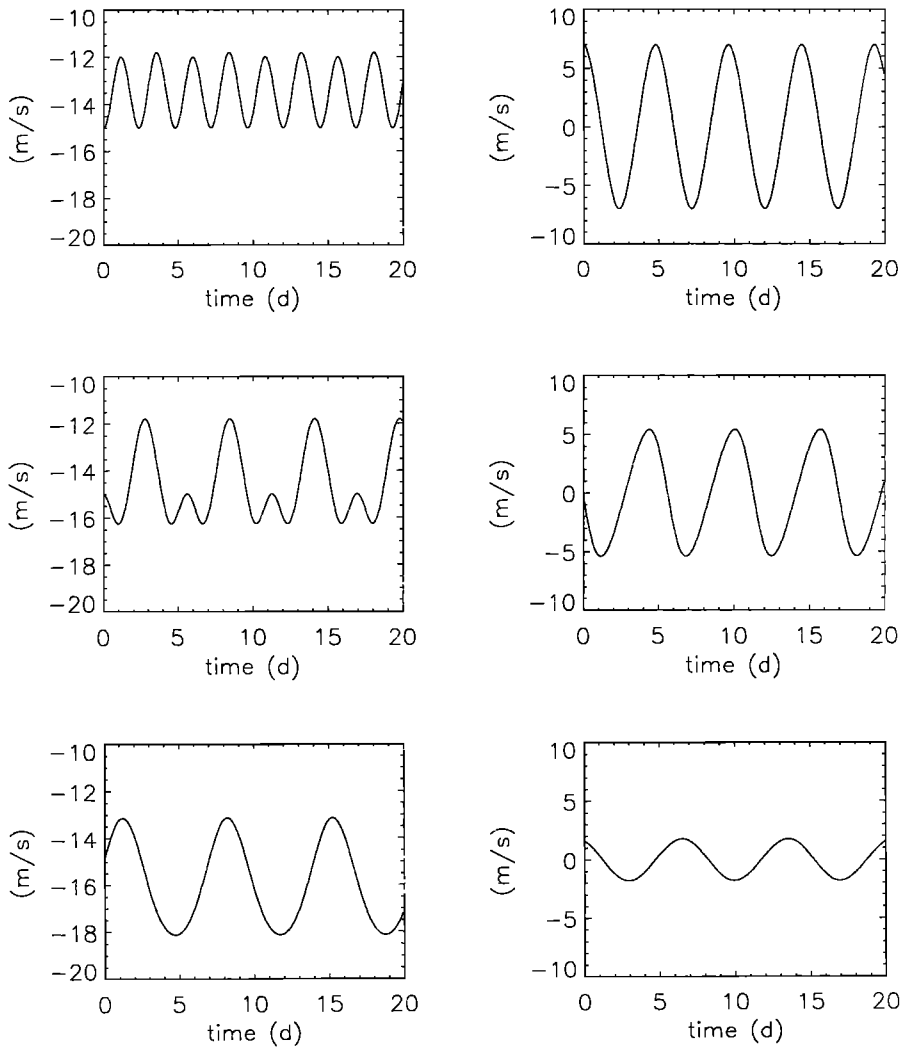

Figure 11. Simulated zonal (left) and meridional (right) wind measured by Balloon 1 (top), Balloon 2 (middle), and Balloon 3 (bottom).

displayed in Plate 3. Also represented are the same quantities for ECMWF interpolated to the time and horizontal position of the SPB observations but at 50 and 70 hPa, i.e., at the analysis levels flanking the SPB-drifting altitude.

Plate 3 shows large differences between instantaneous SPB and ECMWF values. During some periods, the SPB1 zonal winds are close to the corresponding values from the ECMWF analyses at the balloon level (e.g., around day 240). During other periods however, SPB1 winds are closer to ECMWF values at the horizontal balloon location but either at 50 hPa (e.g., around day 249) or at 70 hPa (e.g., around day 242). SPB1 winds show much more features than ECMWF winds, which cannot be simply explained by the different time resolutions. On the other hand, the time mean of ECMWF zonal winds at the SPB1 altitude (-14.5 m s^{-1}) is close to that estimated by the balloon data (-12.1 m s^{-1}). The 2.4 m s^{-1} difference could be partly explained by the balloon Stokes drift: since planetary waves in the equatorial stratosphere are somewhat misrepresented in the ECMWF analyses, real and simulated trajectories differ, and the sampling of the ECMWF zonal velocity at the balloon positions is not expected to produce a Stokes drift that matches the observations.

Regarding the meridional winds, instantaneous balloon and analysis values exhibit once again quite large differences, but they tend to be close to each other at the balloon drifting level. Both time means for meridional wind are very close to 0 m s^{-1} (0.3 m s^{-1} for SPB and -0.4 m s^{-1} for ECMWF; see section 4.2). However, SPB values show a much larger variability (5.3 m s^{-1} root-mean-square (RMS)) than ECMWF analyses (2.6 m s^{-1} RMS).

Regarding nighttime temperatures, SPB1 and ECMWF values are in relatively fair agreement, with a mean difference of only 1 K. Nevertheless, once again, there are episodic events during which the differences between instantaneous values can be as large as 5 K (e.g., around day 254).

Figure 12 presents these comparisons in the form of histograms. The distribution for the meridional wind is rather flat while that for the zonal wind is more peaked and has a positive bias, with ECMWF winds being greater than SPB winds, as we already have seen. The temperature differences are mainly distributed in the range -6 K to $+3$ K but show a

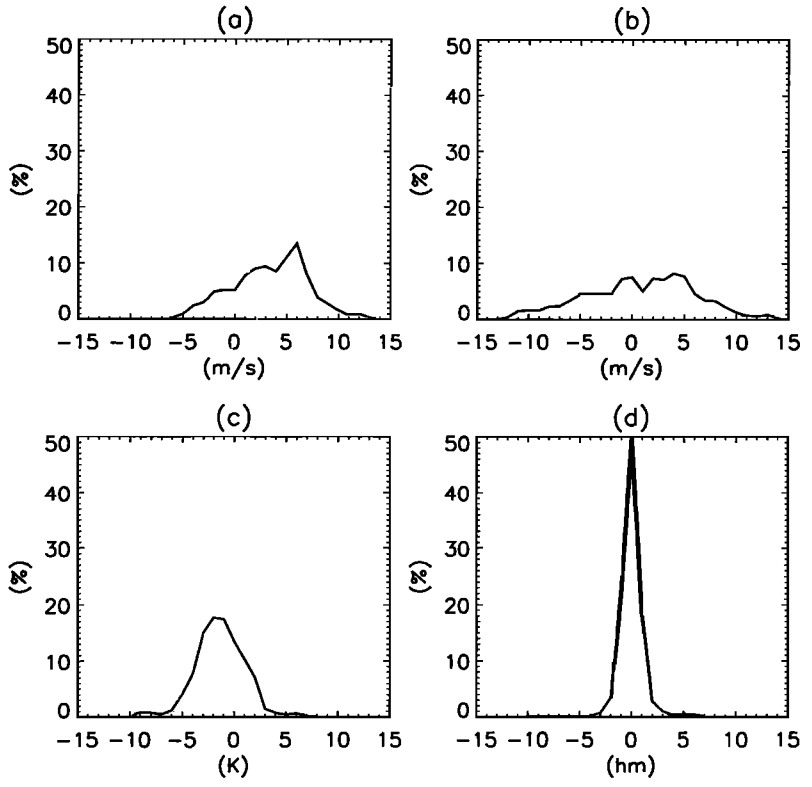

Figure 12. Histograms of the difference (SPB1 – ECMWF) for (a) zonal wind, (b) meridional wind, (c) nighttime temperature, and (d) geopotential height.

negative bias (ECMWF temperatures are warmer than those in the balloon data set). The real bias could be larger, however, because air is warmed at the surface of the gondola (see section 2.2). Nevertheless the dispersion of the distribution is clearly associated with atmospheric fluctuations not captured by the analysis, as can be seen in Figure 3. For the altitude, we plot the differences between the GPS values and the ECMWF geopotential heights. The altitude distribution is symmetric about the origin (no difference in mean) and its dispersion is more probably due to GPS noise.

It thus appears that the mean winds and temperatures are quite well captured by the ECMWF analysis (at least at the SPB drifting levels). On the other hand, the large horizontal wind fluctuations estimated by the SPBs are largely underestimated (or are even absent) in ECMWF analysis particularly for the meridional wind.

To further examine the large-scale waves in the analysis fields, we make a space-time spectrum analysis of the ECMWF meridional wind fields at 70 and 50 hPa between August 25 and October 23, 1998 [*Hayashi*, 1971]. The meridional winds were first decomposed in zonal harmonics. For each harmonic the obtained time series was analyzed by the lag-correlation method using a Hanning spectral window. The number of degrees of freedom is given by $r = 2.67N/M$ where N is the total number of samples and M is the lag number. Here $N = 240$ (60 days x 4) and $M = 120$, so $r = 5.34$. This number of degrees of freedom places the 95% confidence limits of a unit power spectral estimate between 0.42 and 6.43.

Figure 13 shows that the westward moving disturbances that induce meridional wind variability at 70 hPa are dominated by oscillations with zonal wave numbers between 3 and 5 and periods around 4 days. This feature is consistent with the 4-day mixed Rossby-gravity wave. The amplitude of this disturbance (at maximum 3 m s^{-1} on the meridional wind at the equator), however, is much weaker than that estimated from radiosonde data. The picture is essentially the same at 50 hPa (not shown).

6. Summary

In this section we summarize the information on periodic signals provided by the spectral and wavelet analyses of SPB data, as complemented by the results of radio sounding analysis and idealized trajectory calculations.

6.1. Oscillations With an Apparent Period of About 4 Days

The strongest periodic signal in SPB data during the Ecuador campaign was obtained in the meridional wind estimated by SPB2 between days 250 and 260, when the balloon was above the central equatorial Pacific. The intrinsic and apparent periods of that signal were around 6 and 4 days, respectively. Also, between days 250 and 260, the meridional wind estimated by SPB1 and SPB5 over the western and eastern Pacific, respectively, showed strongest activity at intrinsic periods longer than 5 days. The companion signals in the estimated zonal winds had intrinsic periods of about 3 days.

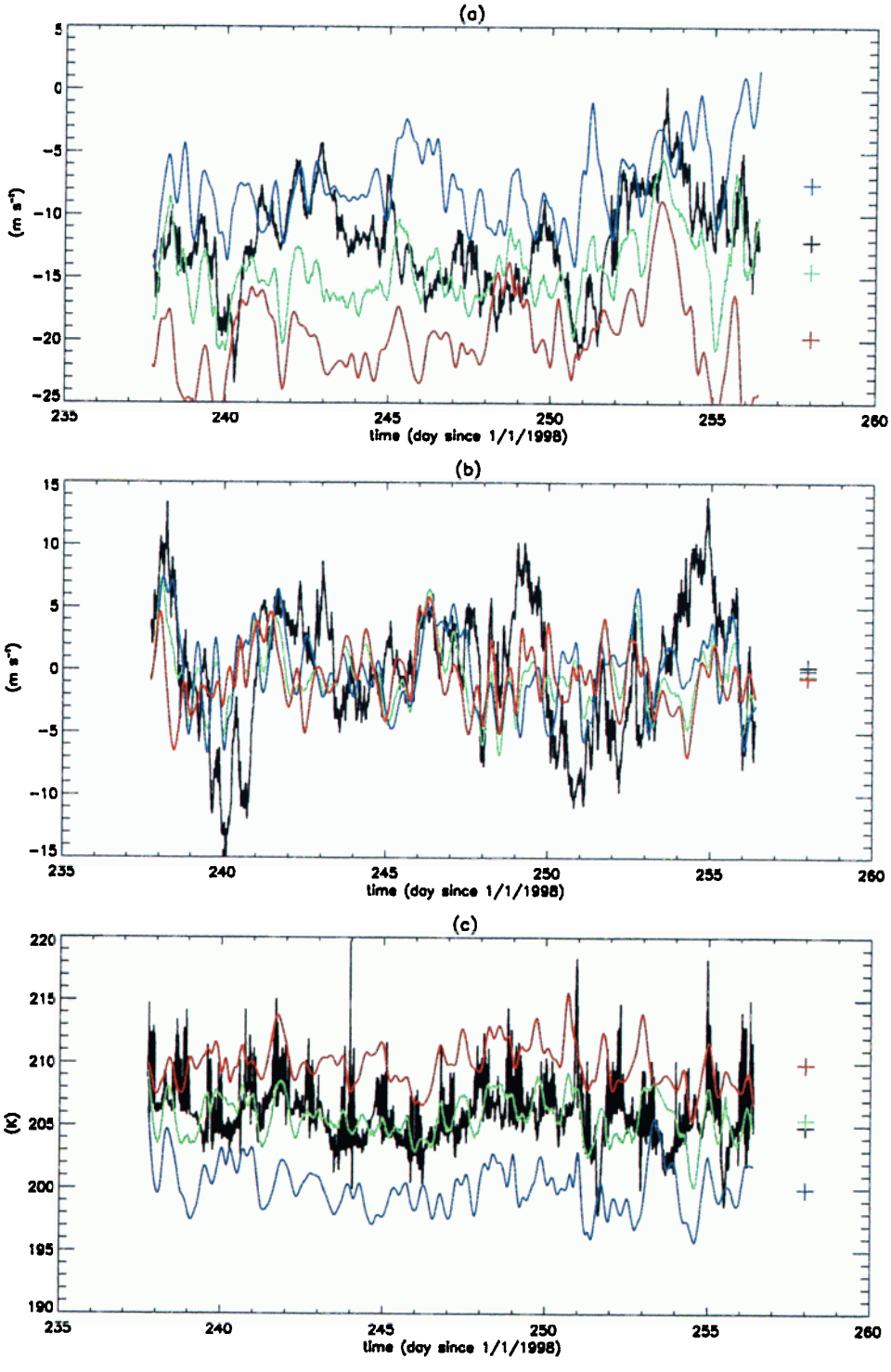

Plate 3. Comparisons between SPB1 (black) with ECMWF-interpolated fields at the balloon level (green), 70 hPa (blue), and 50 hPa (red). (a) Zonal wind, (b) meridional wind, (c) temperature. Note that temperature observations during daytime are invalid (see text). The pluses on the right of the plot represent the mean of the time series.

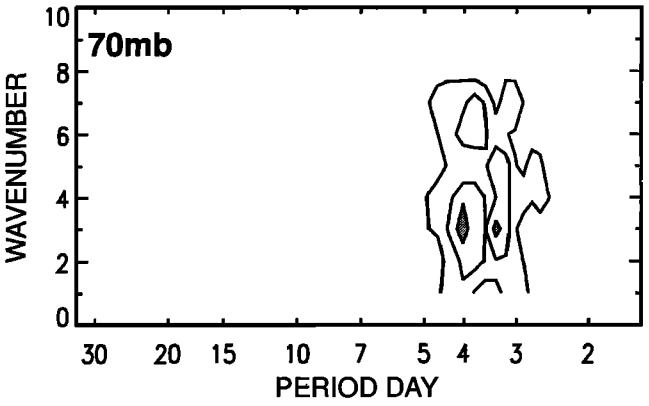

Figure 13. Wave-number-frequency diagram of power spectra multiplied by frequency at the equator for the meridional wind (westward moving waves) from ECMWF analysis. Contour interval: 0.06 m^2 s^{-2}.

Differences between intrinsic periods of the two horizontal wind components are expected if the trajectories cross the equator. Analysis of meridional winds from radiosonde data captured a 4-day wave with the characteristics of a mixed Rossby-gravity wave [*Yanai and Maruyama*, 1966].

These results thus suggest that between Julian days 250 and 260 (i.e., September 7–17, 1998) the lower stratosphere over the equatorial Pacific was affected by a mixed Rossby-gravity wave with the characteristics summarized in Table 2. Our estimate for the vertical wavelength of this wave is 2.5 km (equation (12)). The corresponding estimate by *Yanai and Maruyama* [1966] was 4–6 km. Note, however, that the Ecuador campaign developed during the easterly phase of the QBO, while the work of *Yanai and Maruyama* [1966] was for a period during the westerly phase of the QBO.

The data from SPB1 also suggest that a mixed Rossby-gravity wave event was developing over the first five days of its flight. No similar event was detected either by SPB1 or SPB2 during days 245–250, or by SPB5 after day 260. These considerations suggest that the mixed Rossby-gravity waves in the equatorial lower stratosphere may undergo periods of amplification. In such a scenario the close superposition of balloon trajectories west of South America results from a coincidental agreement between the wave phases at launching times rather than from a quasi-stationarity of the wave. Recently, *Canziani and Holton* [1998] emphazised hints of such a sporadic behavior of planetary-wave activity in the equatorial lower stratosphere.

6.2. Periods Longer Than 6 Days

The clearest periodic signal in the zonal wind estimated by SPB2 was at intrinsic periods in the 6 to 8-day range (or even longer). Traces of activity at these periods were also found in the pressure. This long-period signal corresponds to the spectral peak around 0.1 cycle d^{-1} in SPB2 data.

Analysis of zonal winds from radiosonde data also captured a 10-day wave with the characteristics of a Kelvin wave with zonal wave number 1 [*Wallace and Kousky*, 1968]. The amplitude of the zonal-wind fluctuations at the equator associated with this wave reached ≈ 5 m s^{-1} during periods of enhanced activity. The characteristics of this mode are also summarized in Table 2.

The power spectra of the SPB2 horizontal wind is consistent with a scenario in which, at periods longer than 10 days, the lower stratospheric dynamics is dominated by the QBO and by long-period Kelvin waves. However, the decrease of the pressure spectral power at these low frequencies for this flight suggests that such long-period Kelvin waves had a weak amplitude during the study period. Note however, that the technique used to compute the spectra may artificially reduce the amplitude of the first 2 or 3 spectral points.

6.3. Higher-Frequency Oscillations

Periodic signal with intrinsic periods between 2 and 4 days were also found on the meridional wind estimated by the SPBs. At the latitudes where they have been reported, those waves have little (or even no) signature in the zonal wind and pressure. These waves are thus most probably induced by higher-frequency Rossby-gravity or higher-order Rossby modes. The radio sounding frequency (twice daily at best) did not allow us to clearly identify those high-frequency waves in the analysis made in section 5.1.

Some of these oscillations were captured by two balloons at the same time but at geographically different locations. For instance, the 2-day signal is visible on the SPB2 and SPB5 wavelet analyses around day 271, when the former was over western Africa–eastern Atlantic, and the latter over the western Pacific. We tentatively identify this signal as the "quasi-2-day" Rossby-gravity wave with zonal wave number 3 discussed by, for example, *Salby* [1981] and *Rodgers and Pratta* [1981].

7. Final Remarks

We have analyzed the data set provided by three superpressure balloons drifting in the lower stratosphere after their

Table 2. Planetary-Wave Characteristics During the Ecuador Campaign

Mode	Period		Planetary Wave Number	Vertical Wavelength[a]	Phase Speed	Maximum Amplitude
	Intrinsic	Ground Based				
Rossby-gravity wave	6 d	3.5 d	4	2.5 km	-34 m s^{-1}	$v'_{equator} \approx 10$ m s^{-1}
Kelvin wave	8 d	11 d	1	15 km	43 m s^{-1}	$u'_{equator} \approx 5$ m s^{-1}

[a] Computed by application of the appropriate dispersion relationship.

release from Latacunga (Ecuador) in late August and early September 1998. We showed that the balloon behavior in the large scales can be explained by the combined effects of the zonal-mean flow and planetary waves. In particular, we found the signature of mixed Rossby-gravity and Kelvin waves, which were invoked by *Holton and Lindzen* [1972] to force the easterly and westerly phases of the QBO.

Having data from only three balloons during a limited period of time required to complement the analysis with radiosonde data. Nevertheless, the balloon trajectories provided a pictorial view of parcel behaviors near the equator in the lower stratosphere when planetary waves were present. ECMWF analyses for the period of the Ecuador campaign at the SPBs drifting level closely captured zonal-mean winds and temperatures but severely underestimated fluctuations particularly in the meridional wind.

The encouraging performance of the new Stratéole SPB developed by CNES (the French Space Agency) gives hope on the usefulness of this tool for further studies on the dynamics of lower stratosphere. Part 2 of this paper examines the gravity-wave dynamics and the relevance of those waves for the driving of the QBO.

Appendix A: Wind Estimation by Use of Balloon Trajectories

This appendix presents an estimate of how close the balloon velocity deduced from two consecutive GPS points represents the horizontal wind during that interval. A complete presentation of the tracer-motion equation in a fluid can be found in the work of *Babiano et al.* [2000]. A slightly simplified form that we use for the balloon motion is

$$m_b \frac{d\vec{v}}{dt} = -\frac{1}{2} m_a \left(\frac{d\vec{v}}{dt} - \frac{D\vec{u}}{Dt}\right) - \frac{1}{2}\rho_a C_a A_b \mid \vec{v} - \vec{u} \mid (\vec{v} - \vec{u}) + m_a \frac{D\vec{u}}{Dt} + (m_b - \rho_a V_b)\vec{g}\,, \tag{A1}$$

where m_a is the mass of air displaced by the balloon, m_b is the mass of the balloon system (i.e., envelope, lifting gas, and gondola), ρ_a is the air density at drifting level, $\vec{u}$ is the wind velocity, $\vec{v}$ is the balloon velocity, A_b is the balloon cross-sectional area, C_a is the drag coefficient, and V_b is the balloon volume. The terms on the right-hand side represent the added mass, the drag force, the force exerted by the undisturbed flow on the balloon, and the buoyancy force.

In equation (A1), $\frac{D\vec{u}}{Dt}$ is the time derivative along the path of a fluid element, whereas $\frac{d\vec{u}}{dt}$ is the time derivative along the balloon trajectory. For now, let us assume, as it is generally done, that we can write

$$\frac{D\vec{u}}{Dt} = \frac{d\vec{u}}{dt}\,. \tag{A2}$$

Thus assuming that the balloon is neutrally buoyant ($m_b = m_a = \rho_a V_b$) and that its volume is constant, the horizontal component of equation (A1) can be written as follows:

$$\frac{d(\vec{v} - \vec{u})}{dt} = -L_c^{-1} \mid \vec{v} - \vec{u} \mid (\vec{v} - \vec{u})\,, \tag{A3}$$

where $L_c = \frac{3m_a}{\rho_a C_a A_b}$ is a characteristic length for the balloon. For a spherical balloon, $L_c = \frac{4R'}{C_a}$, where R' is the balloon radius. With $C_a \approx 0.5$ and $R' = 5$ m, we obtain that $L_c \approx 40$ m. Equation (A3) can be integrated twice to obtain the geographical separation Δx between the balloon and the air mass after some time interval Δt:

$$\Delta x = L_c \ln\left(1 + \frac{|\vec{v} - \vec{u}|_{t=0}\,\Delta t}{L_c}\right)\,, \tag{A4}$$

which only depends on the modulus of the velocity difference at the initial time. A difference of that type can be produced by high-frequency motions of the balloons, such as a rapid change of drifting level or horizontal wind bursts.

At the very beginning of the flight the sampling interval between two measurements was 60 s, which allows for resolving the natural oscillation of the balloon when it arrives at its drifting level. The period associated with these oscillations was $180 - 240$ s. This is a little shorter than the Brunt-Väisälä period since the balloon volume stays practically constant during the oscillations, whereas the Brunt-Väisälä period corresponds to adiabatic motions. The vertical excursions due to the natural oscillations of the balloon were rapidly damped and reached a maximum amplitude of ≈ 0.5 hPa, yielding fluctuations of the horizontal wind of ≈ 0.5 m s^{-1}. Accordingly, after 12 min the separation between the balloon and the air mass is ≈ 90 m, i.e., less than the GPS accuracy.

Babiano et al. [2000] have examined the motion of small particles in a fluid in the framework of laboratory experiments, i.e., at small Reynolds numbers. In this case, the drag force in equation (A1) is linear in $\vec{v} - \vec{u}$. They show that taking explicitly into account the difference between $\frac{D\vec{u}}{Dt}$ and $\frac{d\vec{u}}{dt}$ can lead to large discrepancies between $\vec{v}$ and $\vec{u}$. In particular, this is likely to happen near hyperbolic points of the fluid (i.e., when the strain dominates the vorticity).

Following their approach, we can write the new equation of the balloon motion in the form

$$\frac{d(\vec{v} - \vec{u})}{dt} = -\left(J + L_c^{-1}|\vec{v} - \vec{u}|I\right)(\vec{v} - \vec{u})\,, \tag{A5}$$

which is equivalent to their equation (8), and where I and J, respectively, are the identity and the Jacobian matrix:

$$J = \begin{pmatrix} \partial_x u_x & \partial_x u_y \\ \partial_y u_x & \partial_y u_y \end{pmatrix}\,, \tag{A6}$$

with $\vec{u} = (u_x, u_y)$.

Therefore the balloon velocity may differ from the wind velocity if the eigenvalues of J are of the same (or higher) order than $L_c^{-1}|\vec{v} - \vec{u}|$. The eigenvalues of J depend on the horizontal strain, shear, and vorticity of the flow [*Babiano et al.*, 2000]. In the lower stratosphere, these quantities are primar-

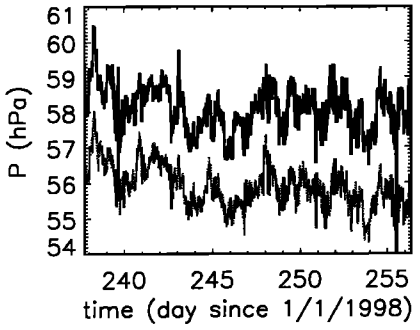

Figure B1. Atmospheric pressure (black) measured by SPB1 and corrected pressure P_a^{corr} (grey) for the same balloon. Note that $P_a^{\text{corr}} - 2$ hPa is actually plotted.

ily controlled by the largest horizontal scales [e.g., *Sheperd et al.*, 2000]. Accordingly, the modulus of the eigenvalues of J are of the order of some 10 m s^{-1} per 1000 km. Therefore one can make the assumption in equation (A2) as long as

$$|\vec{v} - \vec{u}| \gg 10^{-4}\,\text{m s}^{-1}\,. \tag{A7}$$

Moreover, if $|\vec{v} - \vec{u}|$ becomes close to 10^{-4} m s^{-1}, equation (A5) shows that the balloon and the air velocities may diverge, but in this case, the drag force will dominate J and will restore $|\vec{v} - \vec{u}| \sim 10^{-4}$ m s^{-1}. The balloon velocity therefore represents the wind velocity to some of 10^{-4} m s^{-1}. This critical value obviously leads to less uncertainty on air velocity than the GPS measurements.

Appendix B: Balloon Behavior under Changes in Superpressure

The balloon volume (and thus the drifting level) is controlled by the superpressure (See equation (3)). The helium pressure (and temperature) inside the envelope is primarily determined by the envelope temperature. Thus absorption of solar radiation by the envelope during daytime leads to helium warming, balloon expansion, and increase of the drifting level. Most of the absorption bands of the material that forms the envelope are, however, in the infrared. Therefore the superpressure can also change due to changes in impinging long-wave radiation (such as the passage of the balloon over very cold superclusters). Second, the superpressure may also change due to atmospheric pressure variations on an isopycnic surface (if, for instance, the balloon encounters a disturbance). Thus balloon motions are not truly isopycnic. Nevertheless, the departures from a pure isopycnic behavior is quite small, as we show in this appendix.

Laboratory studies have shown that changes in balloon diameter (D) and in superpressure (P_s) are linked through

$$\Delta D = \alpha_D \Delta P_s\,, \tag{B1}$$

where Δ means variations, and α_D is a coefficient that depends on temperature ($\alpha_D = 6.7\,10^{-5}$ m Pa^{-1} at the temperature encountered by the SPBs: $T \approx 200$ K). The changes in balloon volume (V) and P_s are therefore linked through

$$\frac{\Delta V}{V} = 3\alpha_D \frac{\Delta P_s}{D} = -\frac{\Delta \rho_h}{\rho_h}\,, \tag{B2}$$

where ρ_h is the helium density. Furthermore, since the mass of the balloon and gondola are constant, changes in the helium density and surrounding air density (ρ_a) verify

$$\frac{\Delta \rho_h}{\rho_h} = \frac{\Delta \rho_a}{\rho_a}\,. \tag{B3}$$

Suppose first that the helium temperature (and thus the superpressure) is changing. Then the change in drifting level is simply given by (B2):

$$\frac{\Delta \rho_a}{\rho_a} = -3\alpha_D \frac{\Delta P_s}{D} \approx \frac{\Delta P_a}{P_a}\,, \tag{B4}$$

where P_a is the atmospheric pressure and where we have assumed that at least locally, the lower stratospheric temperature is constant. With $D = 10$ m, an observed $\Delta P_s \approx 5$ hPa (see Figure 4 at sunset and sunrise) and a background temperature of ≈ 200 K, equation (B4) yields $\frac{\Delta P_a}{P_a} \approx -0.01$. Thus $\Delta P_a \approx -0.6$ hPa (i.e., $\Delta P_a \approx -0.1 \Delta P_s$), which agrees with the diurnal cycle on pressure measurements.

Consider now that pressure changes (ΔP_a) on an isopycnic surface. The superpressure change is simply $\Delta P_s = -\Delta P_a$. This superpressure change causes the balloon to make an additional vertical displacement $\Delta P_e \approx -0.1 \Delta P_s$, as previously. Indeed, if the balloon ascends (descends) due to the wave, $\Delta P_a < 0$ ($\Delta P_a > 0$) and the superpressure increases (decreases), causing a little additional ascent (descent).

These estimates enable us to correct the superpressure changes effect. If $\bar{P}_s$ is the mean superpressure during the flight, the quantity

$$P_a^{\text{corr}} = P_a + 0.1(P_s - \bar{P}_s) \tag{B5}$$

will be void of residual changes in balloon volume due to superpressure changes. For instance, the spectrum of P_a^{corr} for SPB2 (not shown) does not exhibit a peak at the 24-hour period. However considering P_a^{corr} rather than P_a has one disadvantage: the noise in P_a^{corr} is larger than in P_a since it includes the noise of P_s. Therefore in the remainder of the text (as well as in part 2 of this paper), the results presented are based on P_a. Nevertheless, we have checked that the results do not depend on the choice of P_a or P_a^{corr}. This is emphasized in Figure B1, which shows the atmospheric pressure measured by SPB1 and the associated P_a^{corr}. The figure actually shows $P_a^{\text{corr}} - 2$ hPa since the difference between P_a and P_a^{corr} is very small.

Finally, we note that the correction given by equation (B5) is not sufficient for SPB5. It appears that the atmospheric pressure sensor of this balloon was not well calibrated, which induced it to overestimate the pressure changes during day/night transitions (i.e., when the temperature of the sensor itself exhibits large changes).

Acknowledgments. This study was made in the framework of the Stratéole/Vorcore Project. One of us (C.R.M.) was also supported by the U.S. NSF grant ATM-9630225. We would like to thank all the Vorcore project members for helpful discussions at different stages of this study. Maman Sudarisman from the Indonesian Meteorological Office participated in the analysis of the radio sounding data when preparing his Diplôme d'Études Approfondies in France. Figure 13 was produced by J.-H. Jung. The authors gratefully acknowledge the CNES launching and operation team at Latacunga for the successful balloon flights.

References

Andrews, D. G., J. R. Holton, and C. B. Leovy, *Middle Atmosphere Dynamics*, Academic, San Diego, Calif., 1987.

Babiano, A., J. H. E. Cartwright, O. Piro, and A. Provenzale, Dynamics of a small neutrally buoyant sphere in a fluid and targeting in Hamiltonian systems, *Phys. Rev. Lett. B*, *84*, 5764–5767, 2000.

Canziani, P. O., and J. R. Holton, Kelvin waves and the quasi-biennial oscillation: An observational analysis, *J. Geophys. Res.*, *103*, 31,509–31,521, 1998.

Carli, B., et al., Minor constituent concentrations measured from a high altitude aircraft using high resolution far-infrared Fourier Transform spectroscopy, *J. Atmos. Chem.*, *35*, 273–293, 2000.

Desbois, M., Large-scale kinetic energy spectra from Eulerian analysis of Eole wind data, *J. Atmos. Sci.*, *32*, 1838–1847, 1975.

Dowden, R. L., and R. H. Holzworth, Longitudinal variation of midlatitude hiss from six long duration balloon flights, *J. Geophys. Res.*, *95*, 10,599–10,607, 1990.

Dubourg, V., F. Nouel, and M. Durand, Pressurised balloon systems: Results of Ecuador 1998 and Theseo 1999, in *Proceedings of 14th ESA Symposium on European Rocket and Balloon Programmes and Related Research*, ESA SP-437, pp. 105–110, Eur. Space Agency, Noordwijk, The Netherlands, 1999.

Dunkerton, T. J., Inferences about QBO dynamics from the "tape recorder" effect, *J. Atmos. Sci.*, *57*, 230–246, 2000.

Giles, J. K., and J. K. Angell, A southern hemisphere horizontal sounding system, *Bull. Am. Meteorol. Soc.*, *44*, 687–696, 1963.

Hayashi, Y., A generalized method of resolving disturbances into progressive and retrogressive waves by space Fourier and time cross-spectral analyses, *J. Meteorol. Soc. Jpn.*, *49*, 125–128, 1971.

Hertzog, A., and F. Vial, A study of the dynamics of the equatorial lower stratosphere by use of ultra-long-duration balloons, 2. Gravity waves, *J. Geophys. Res.*, this issue.

Holton, J. R., and R. S. Lindzen, An updated theory for the quasi-biennial cycle of the tropical stratosphere, *J. Atmos. Sci.*, *29*, 1076–1080, 1972.

Holzworth, R. H., K. W. Norville, H. Hu, R. L. Dowden, C. D. D. Adams, J. Brundell, O. Pinto Jr., I. Pinto, and W. D. Gonzalez, Extended life balloon-borne observatories, *Radioscientist*, *4*, 33–37, 1993.

Julian, P., V. E. Lally, W. Kellogg, and V. Suomi, The TWERL Experiment, *Bull. Am. Meteorol. Soc.*, *58*, 936–948, 1977.

Kalnay, E., et al., The NCEP/NCAR 40-year reanalysis project, *Bull. Am. Meteorol. Soc.*, *77*, 437–471, 1996.

Lally, V. E., Satellite satellites: a conjecture on future atmospheric sounding systems, *Bull. Am. Meteorol. Soc.*, *41*, 429–432, 1959.

Malaterre, P., V. Dubourg, G. Letrenne, and M. Durand, The long duration "MIR" balloon, in *Proceedings of 12th ESA Symposium on European Rocket and Balloon Programmes and Related Research*, ESA SP-370, pp. 329–334, Eur. Space Agency, Noordwijk, The Netherlands, 1995.

Mallat, S., *A Wavelet Tour of Signal Processing*, Academic, San Diego, Calif., 1998.

Mariotti, A., M. Moustaoui, B. Legras, and H. Teitelbaum, Comparisons between vertical ozone soundings and reconstructed potential voticity maps by contour advection with surgery, *J. Geophys. Res.*, *102*, 6131–6142, 1997.

Mariotti, A., C. R. Mechoso, B. Legras, and V. Daniel, The evolution of the ozone"collar" in the antarctic lower stratosphere during early August 1994, *J. Atmos. Sci.*, *57*, 402–414, 2000.

McIntyre, M. E., and T. N. Palmer, The 'surf zone' in the stratosphere, *J. Atmos. Sol. Terr. Phys.*, *46*, 825–849, 1984.

Morel, P., and W. Bandeen, The EOLE experiment: Early results and current objectives, *Bull. Am. Meteorol. Soc.*, *54*, 298–306, 1973.

Percival, D. B., and A. T. Walden, *Spectral Analysis for Physical Applications*, Cambridge Univ. Press, New York, 1993.

Plumb, R. A., D. W. Waugh, R. J. Atkinson, P. A. Newman, L. R. Lait, M. R. Schoeberl, E. V. Browell, A. J. Simmons, and M. Loewenstein, Intrusions into the lower stratospheric Arctic vortex during the winter of 1991–1992, *J. Atmos. Sci.*, *99*, 1089–1105, 1994.

Pommereau, J. P., and A. Hauchecorne, A new atmospheric vehicle: La Montgolfière infrarouge, *Adv. Space Res.*, *1*, 55–60, 1980.

Rodgers, C. D., and A. Pratta, Evidence for a 2-day wave in the middle atmosphere, *J. Geophys. Res.*, *86*, 9661–9664, 1981.

Salby, M. L., The 2-day wave in the middle atmosphere: Observations and theory, *J. Geophys. Res.*, *86*, 9654–9660, 1981.

Sheperd, T. G., J. N. Koshyk, and K. Ngan, On the nature of large-scale mixing in the stratosphere and mesosphere, *J. Geophys. Res.*, *105*, 12,433–12,446, 2000.

Sitbon, P., Platform location and data collection by satellite systems, *IEEE Trans. Geosci. Electr.*, *13*, 2–17, 1975.

Solot, S. B., and J. K. Angell, The mean upper air flow in the southern hemisphere temperate latitudes determined from several years of GHOST balloons flights at 200 and 100 mb, *J. Atmos. Sci.*, *30*, 3–12, 1973.

Vial, F., et al., STRATÉOLE: A project to study Antarctic polar vortex dynamics and its impact on ozone chemistry, *Phys. Chem. Earth*, *20*, 83–96, 1995.

Wallace, J. M., and V. E. Kousky, Observational evidence of Kelvin waves in the tropical stratosphere, *J. Atmos. Sci.*, *25*, 900–907, 1968.

Yanai, M., and T. Maruyama, Stratospheric wave disturbances propagating over the equatorial Pacific, *J. Meteorol. Soc. Jpn.*, *44*, 291–294, 1966.

C. Basdevant, A. Hertzog, and F. Vial, Laboratoire de Météorologie Dynamique, École Polytechnique, F-91128 Palaiseau Cedex, France. (basdevan@lmd.ens.fr; hertzog@lmd.polytechnique.fr; vial@lmd.polytechnique.fr)

C. R. Mechoso, Department of Atmospheric Sciences, University of California, Box 951565, Los Angeles, CA 90095-1565. (mechoso@atmos.ucla.edu)

P. Cocquerez, V. Dubourg, and F. Nouel, Centre National d'Études Spatiales, 18 avenue Édouard Belin, 31401 Toulouse Cedex 4, France. (cocquerez@cnes.fr; dubourg@cnes.fr; nouel@cnes.fr)

(Received December 8, 2000; revised May 22, 2001; accepted May 25, 2001.)